Optics & Laser Technology 153 (2022) 108216

Contents lists available at ScienceDirect

Optics and Laser Technology

journal homepage: www.elsevier.com/locate/optlastec

Effect of laser processing parameters and carbon black on morphological and mechanical properties of welded polypropylene

Foram Dave [a,b,*], Muhammad Mahmood Ali [a,b], Mozaffar Mokhtari [c], Richard Sherlock [b,d], Alistair McIlhagger [e], David Tormey [a,b]

[a] Department of Mechanical and Manufacturing Engineering, Atlantic Technological University Sligo, Ash Lane, F91 YW50 Sligo, Ireland
[b] Centre for Precision Engineering, Materials and Manufacturing (PEM) Centre, Atlantic Technological University Sligo, Ash Lane, F91 YW50 Sligo, Ireland
[c] National Graphene Institute and Department of Materials, School of Natural Sciences, The University of Manchester, Oxford Road, Manchester, M13 9PL, United Kingdom
[d] Department of Life Sciences, School of Science, Atlantic Technological University Sligo, Ash Lane, F91 YW50 Sligo, Ireland
[e] School of Engineering, Ulster University, Newtownabbey BT37 0QB, UK

ARTICLE INFO

Keywords:
Laser transmission welding (LTW)
Carbon black (CB)
Thermal characterisation
Polymer crystallinity
Weld lap shear strength
Optimisation in laser technology

ABSTRACT

In the present work, laser process window and welding suitability of the neat isotactic polypropylene (iPP) and its carbon black (CB: 0–3 wt.%) composites was defined for laser transmission welding (LTW) with the help of thermal characterisation and thermal simulation. This novel approach of welding feasibility moves from trial and error to robust analytical methods. The non-contact spacer method is also a novel feature of this study, followed by X-ray diffraction of the laser-treated iPP composites. This study emphasises the importance of crystallinity in defining weld integrity and quality. The welding experiments were conducted with line energies of 0.06–0.12 J/mm using the Response Surface Methodology approach by varying laser power and welding speed. The composites with 0.5 wt.% and 1.0 wt.% of CB were welded successfully with neat iPP, but composites with CB (>1 wt.%) were difficult to weld due to degradation. Weld lap shear strength and apparent weld width measured during mechanical testing showed better weld quality for 1 wt.% CB welded at line energy 0.12 J/m. Mathematical models have been developed based on the experimental results of central composite design after backward elimination. The present study demonstrates that an increase in CB to an optimised value fulfils the requirements of high welding speed with improved crystallinity and weld strength. This study is of keen interest to industrialists and researchers.

1. Introduction

Laser transmission welding or LTW is a joining technique to weld two or more plastic surfaces in a selective and contactless manner with low mechanical and thermal stresses [1]. It is a clean and precise electromagnetic welding process amenable to a high degree of automation [2]. In this process, there is no pre-treatment requirement (like surface cleaning in adhesive bonding), no mechanical stress accumulation (like in ultrasonic or vibration welding) and no generation of micro-particles or any by-products [3]. The application of LTW of plastics has increased with the development of high power diode lasers emitting at wavelengths in the near-infrared [4]. The joints formed through diode laser welding are cleaner and stronger[5]. During the process, the radiation passes through the laser transmissive layer (L_T) and hits the laser absorptive layer (L_A), which are in close contact with each other with the help of a clamping pressure or force[6,7]. The L_A often contains carbon black (CB), which can absorb the laser energy, converts it into heat energy, and consequently melt the materials, leading to a weld formation at the interfacial regions of the layers. With the LTW technique, precise welding can be possible in hard-to-reach areas [8-10]. CB in L_A

Abbreviations: iPP, isotactic Polypropylene; CB, Carbon Black; LTW, Laser Transmission Welding; L_T, Laser Transmissive Layer; L_A, Laser Absorptive Layer; XRD, X-Ray Diffraction; DSC, Differential Scanning Calorimetry; T_c, Crystallinsation temperature; X_c, Degree of Crystallinity; ΔH_c, Enthalpy of Crystallisation; TGA, Thermogravimetric Analysis; DTG, Derivative Thermogravimetric Analysis; NMR, Nuclear Magnetic Resonance; IR, Infrared Spectroscopy; P, Laser Power; S, Welding Speed; DoE, Design of Experiment; RSM, Response Surface Methodology; CCD, Central Composite Design; ANOVA, Analysis of Variance; WW, Apparent Weld Width; σ, Weld Lap Shear Strength.

* Corresponding author at: Department of Mechanical and Manufacturing Engineering, Atlantic Technological University Sligo, Ash Lane, F91 YW50 Sligo, Ireland.
E-mail addresses: foram.dave@mail.itsligo.ie, foram.dave91@gmail.com (F. Dave).

https://doi.org/10.1016/j.optlastec.2022.108216
Received 3 November 2021; Received in revised form 30 March 2022; Accepted 25 April 2022
Available online 14 May 2022

plays an important role in the LTW process[11]. In 2001, during LTW of polypropylene and polyacetal, Haberstroh et al.[11] studied the influence of CB on weld strength and also carried out the initial analyses of the weld seam cross-section. In 2006, Haberstroh et al. [12] examined the influence of CB loading on the weld seam formation while joining thermoplastics (neat polycarbonate, PC as L_T and PC containing 0.5, 1 and 1.5 wt.% CB as L_A) in micro-technology applications. It has been noticed that, with an increase in the CB content, there was a decrease in the penetration depth. This was due to the change in the type of absorption with an increase in CB, i.e., from volume absorption to surface absorption where weld width is higher than weld depth. The optical penetration depth in the L_A layer is determined by the concentration of CB, which defines the temperature distribution, the shape and strength of the laser welds during the welding process [13]. However, in these studies, the influence of crystallinity was not studied in detail which is the most important characteristic of semi-crystalline polymers that ultimately determine their mechanical properties [14]. Some studies correlate an increase in CB concentration with the crystallinity of iPP due to nucleation promotion [15]. However, these studies do not describe the LTW process with material crystallinity in detail. Ghorbel et al. [16] studied the geometrical and microstructure characterisation of the weld during LTW of iPP, however, its overall influence on the mechanical properties of the welded iPP is not studied in detail. In the present study, we are trying to correlate CB and laser parameters with the crystallinity of iPP and extend this correlation by measuring and analysing the mechanical properties of the laser welded iPP.

The degree of crystallinity differs with polymer grade, compounding ingredients and their processing conditions [17]. In the present study, injection moulded isotactic polypropylene (iPP) is used as the base material which is a semi-crystalline thermoplastic [18]. It is a high-volume commodity plastic often known for its low-cost engineering material. It has good hardness, chemical and environmental stress cracking resistance. Depending upon the percentage of the polymorphic forms α, β, γ and mesomorphic, the percentage of crystallinity in iPP varies, typical range 30–60%. These transformations and degrees of crystallinity can be determined using X-ray diffraction analysis (XRD), Differential Scanning Calorimetry (DSC), nuclear magnetic resonance (NMR) and infrared (IR) spectroscopy. In LTW of plastics, melting energy depends on the crystallinity grade for semi-crystalline thermoplastics. The melting energy is relative to the proportion of the crystalline phase of semi-crystalline polymers.

The mechanical properties of the laser-welded products or the weld quality also depend upon the laser parameters such as laser power (P), welding speed (S), clamping pressure, spot diameter, etc [16,19,20]. P and S are considered the most important parameters of the LTW process. P determines the laser intensity controlling the heat input and S determines the laser-polymer interaction time that controls the heat diffusion during the LTW process [21,22]. The distribution of laser energy within the focus spot can also impact weld quality, but this is not readily adjustable for a given LTW set-up and is considered a constant in this work. A Gaussian beam with a beam diameter of 2.1 mm is used in the present study. Higher P values allow for greater S and decrease the cycle time for better productivity. In one of the studies, Acherjee et al. (2017) [23] welded neat polycarbonate (PC) with 0.1 wt.% CB at P = 10–20 W, S = 4–16 mm/s, the stand-off distance of 25–37 mm and clamp pressure varying from 1.2 to 6 MPa. They observed higher weld strength at higher P values. Mamuschkin et al. (2013) [24] also obtained higher strength (in terms of breaking load) of the laser welded iPP samples at higher values of power of the diode laser. However, excess heat input may lead to partial decomposition of the welding materials leading to the formation of weaker bonds and lower weld shear strength values [25]. In these studies, the degradation temperature of the material was not determined, which plays an important role to understand the weld failure.

Sufficient laser energy is required during LTW to initiate the melting of the polymer. Defining a process window for LTW of thermoplastics and their composites is often challenging due to the inherent non-linearity of the relationship between the input energy parameters and resulting temperature profile and the high heat density of the process [21].

In the present research, injection moulded neat iPP was used as L_T layer and CB incorporated iPP composites (PP-CB) were used as the L_A layer, defined in section 2. The first objective of the present study is to define laser process parameters using preliminary results of thermal simulation and thermal characterisation of the base material without laser welding (section 3). The second objective is to study the trend of the change in the percentage of crystallinity of the laser-treated sample through the non-contact spacer method. This is a novel approach in the morphological study of the LTW of semi-crystalline polymers which defines the effect of the thermal cycle leading to morphological changes and correlating to the mechanical properties of the welds (section 5). To the best of our knowledge, it has not been applied in other published approaches that investigate LTW. This differentiates our approach from what has already been published. Laser trials were carried out based on the results from thermal and morphological studies to achieve the third objective of the present research. The last objective is to investigate the effect of varying CB and laser parameters on the LTW process and weld integrity, which was studied in detail through a design of experiment (DoE) response surface methodology (RSM). The performance of LTW was evaluated through the lap-joint shear test method, which is considered the most suitable test method [26]. Weld quality was analysed in terms of apparent weld width and weld lap shear strength obtained after mechanical testing of lap joint laser-welded composites, as described in section 6. The importance of crystallinity to the overall strength of the laser-welded composite is highlighted as a unique novelty of the present study. The study of the effect of CB % on polymer crystallinity is a distinct dimension of this paper and this is not reported earlier to the best of our knowledge. RSM (details are provided in Supplementary File Note 1) and analysis of variance (ANOVA) was used after backward elimination to develop regression equations for determining an optimised set of process parameters for the LTW of the PP-CB composites described in section 6. Furthermore, regression equations have been obtained to predict apparent weld width and weld lap shear strength using the results of mechanical testing. Emphasising these objectives, the present research article fills the gap and provides a state-of-the-art of importance of CB, crystallinity and laser parameters for defining laser processing window and weld qualities in the field of LTW. The flow chart shown in Fig. 1, represents the optimisation of the laser welding process of the polymers with the aid of experimental, simulation and characterisation of the samples.

2. Materials

In the present work, a neat iPP was used as a laser transmissive layer (L_T) and iPP composites containing 0.5, 1.0, 2.0 and 3.0 wt.% CB were was used as a laser absorptive layer (L_A). These samples have a small percentage of ethylene content (PPCP: random polypropylene copolymer). Rectangular samples of dimension $40 \times 10 \times 2\,mm^3$ were cut from injection moulded plaques of size $76.2 \times 50.8 \times 2\,mm^3$ using a pneumatically operated test sample cutting press with a cutting die. The samples are obtained from industrial partners for research purposes. As shown in Fig. 2, the rectangular samples were stamped from either side of the hole to avoid the effects of formed flow lines of injection moulded parts on welding quality as much as possible. Flow lines are the weak areas for the injection moulded parts. If they are included in the samples that need to be welded, stress will be focused on a small rather than distributed throughout the polymer matrix during application.

3. Methodology for defining laser process window

Thermal analysis of the base material was carried out to determine the melting and degradation temperature. These temperatures were

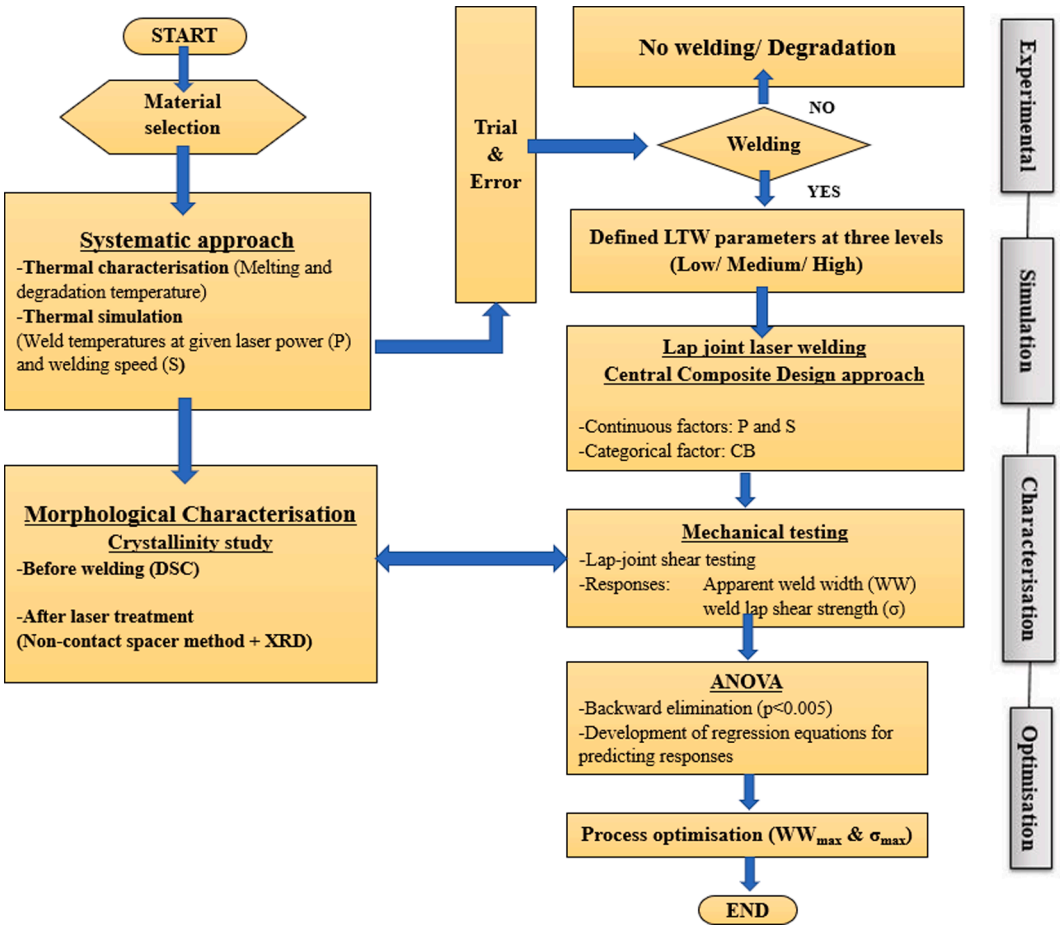

Fig. 1. Flow chart representing the optimisation of the laser welding process of the polymers with the aid of experimental, simulation and characterization of the samples.

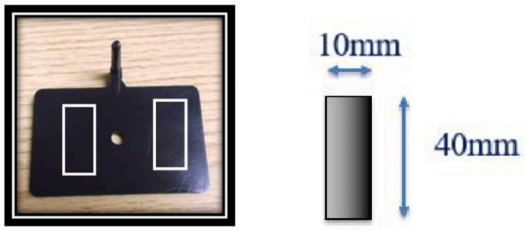

Fig. 2. Region selection for lap joint weld geometry.

correlated with the thermal modelling temperatures and the laser process window was defined.

3.1. Thermal properties of base materials

The samples for thermal analysis were microtomed (Leica SM200 R) to the films with a thickness of 120 μm from the mid-portion/cross-section of the base material, neat iPP and its CB composite before welding trials. All the CB composite (0.5, 1, 2 and 3 wt.%) samples were considered for thermal characterisation.

Thermogravimetric analysis (TGA) was carried out via a Perkin Elmer Pyris TGA 1. The samples were heated from 30 °C to 700 °C at 20 °C/min using an aluminium crucible.

Non-isothermal Differential Scanning Calorimetry (DSC) tests were carried out to investigate the thermal properties of the neat iPP and its composites. The untreated films were heated from −50 °C to 200 °C, held isothermally at 200 °C for 10 min to remove the thermal and stress histories, cooled to −50 °C and then heated up to 200 °C again using a Perkin Elmer DSC4000. The heating rate of the scans was at the rate of 10° C/min. The melt temperatures T_{m2} were determined from the melting peak of the first and second heating scans, respectively. The crystallisation temperature (T_c), its onset (T_{onset}) and enthalpy of crystallisation (ΔH_c) were obtained from the maximum onset and area of the crystallisation peak of the cooling scan. The ratio of the melting enthalpy, ΔH_f from the fourth cycle and the enthalpy of fusion of ideal iPP crystal ($\Delta H_{fo} = 207$ J g-1) was applied to estimate the degree of crystallinity of iPP in the composites (X_c).

Thermal degradation of iPP and its CB composites were studied by determining their mass loss during heating. Fig. 3 shows the mass loss (TG%) and the derivative mass loss (DTG) curves of all the composites. The graph indicates that all the composites showed a single step of degradation. The onset degradation temperature of neat iPP begins at 410.13 °C, while the presence of CB leads to a shift of the initial mass loss towards higher temperature. In the TGA curve (Fig. 3, (a)), there was a clear shift of onset temperature of almost 130 °C for composites containing 0.5 wt.% of CB. In the DTG curve (Fig. 3, (b)), a significant shift of the first derivative peak to a higher temperature with CB was observed. For 0.5 wt.% CB, there was a shift of~ 79 °C in the peak temperature. The results indicate an enhancement in the thermal stability of the composites with an increase in CB content. Similar behaviour of CB nanocomposites was observed by Chrissafis et al., 2007 [27] using the iPP matrix. Higher degradation temperatures are advantageous for the welding process as it facilitates higher temperature welding through larger weld zones and perhaps increases the flow in the melt. Table 1 shows that the temperature during the laser welding process should be below 410 °C to avoid degradation of the welding assembly, which will

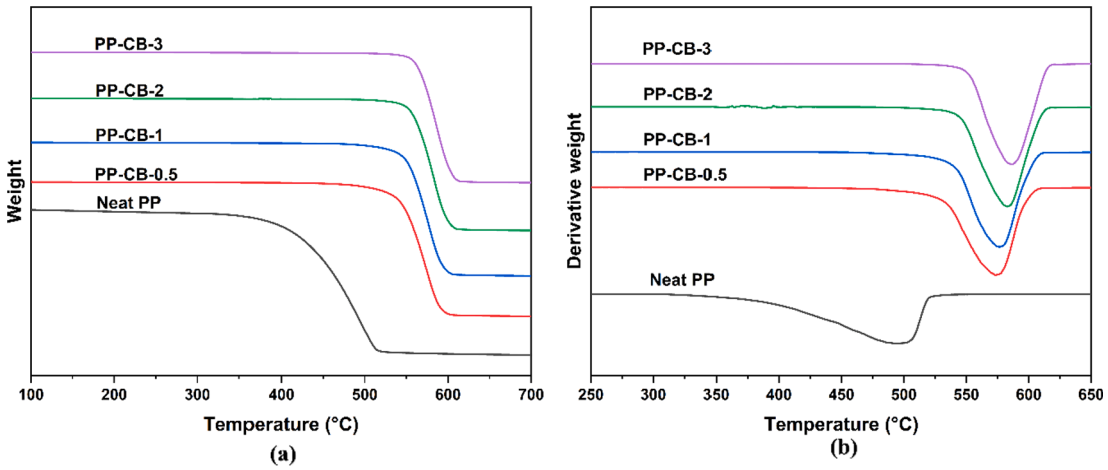

Fig. 3. (a) TGA and (b) DTG traces of PP-CB composites.

Table 1
Results of TGA/DTG traces for PP-CB Composites.

Composites	Onset degradation temperature (°C)	Peak temperature of DTG curve (°C)
Neat PP	410.13	494.71
PP-CB-0.5	540.10	573.62
PP-CB-1	543.49	576.89
PP-CB-2	559.37	582.87
PP-CB-3	566.06	586.50

deteriorate the weld strength.

The laser energy needs to be sufficient to allow the material to melt, flow and inter-diffuse at the interface of the joining assembly. The temperatures obtained from DSC results helps to set the laser parameters. Fig. 4 shows the DSC cooling and heating traces of iPP and its composites. An exothermic transition was observed in the cooling scan (Fig. 4, a) for all the composites due to crystallisation. An increase in the T_{onset} for CB composites compared to neat iPP indicates the nucleation behaviour of CB which increases the crystallinity [28]. The increase in crystallinity leads to an increase in the chain packing of the polymer.

The results of the cooling exotherm are summarised in Table 2. It shows that the T_{onset} of iPP increased by ~10° C at a loading of 0.5 wt.% of CB (PP-CB-0.5). Further increase of CB did not show much change on T_{onset}. For 0.5 wt.% and 1.0 wt.% CB, the rate of crystallisation was faster. T_{m2} is the peak endothermic temperature or the melting temperature from the second heat curve of DSC which was used for calculating $\Delta T = (T_{m2}\text{-}T_c)$. The value of T_{m2} did not vary much upon the incorporation of varying amounts of CB. For 0.5 and 1.0 wt.% of CB, there was a decrease in the value of ΔT, which confirms that CB acts as a nucleating agent for these two compositions and increases the crystallinity of the composite.

The second heat scan (Fig. 4,b) were used to evaluate the melting characteristics of neat iPP and its CB composites and the effect of CB filler. Two melting endotherms were observed for each composite in the second heating scan. This could be due to the melting behaviour of different types of lamellar crystals and crystallite size [29], with melting temperatures around 135 °C and 148 °C. This would have formed due to the presence of a small percentage of ethylene content in iPP (PPCP: polypropylene random copolymer). It could also be due to previous crystallisation conditions, i.e., cooling rate or step-like melting mechanism properties. The decrease in the melting T_{onset} confirms the imperfect crystal formation in the iPP composites with CB content.

Table 2
Results of DSC traces of PP-CB Composites (heating rate 10° C/min, N_2 atm).

Composite designation	T_{onset} (°C)	T_c(°C)	ΔH_c (J/g)	T_{m2}(°C)	ΔT (T_{m2}-T_c)
Neat PP	135.85	115.23	75.08	148.36	33.13
PP-CB-0.5	145.82	115.29	68.08	147.92	32.63
PP-CB-1	149.98	115.00	63.13	148.07	33.07
PP-CB-2	144.01	114.19	78.87	148.05	33.86
PP-CB-3	145.49	114.49	58.39	147.91	33.42

T_{onset}, onset temperature of crystallisation; T_c, peak exotherm temperature; ΔH_c, heat of crystallisation from the area under the exothermic peak; Tm_2, peak endothermic temperature/melting temperature.

The crystallinity percentage (χ_{DSC}) was evaluated as the ratio of measured enthalpy of fusion from the area under the curve of endothermic transition and enthalpy of 100% crystalline iPP as given by equation (1). The enthalpy for 100% crystalline iPP was taken from the literature 207 J/g [30].

$$\chi_c = \frac{\Delta H_f}{\Delta H_{fo}\,(1 - X_p)} X100 \quad (1)$$

The results of melting and percentage crystallinity are summarised in Table 3. Percentage crystallinity was measured from DSC (χ_{DSC}) curves.

Including CB into the iPP, matrix affects its crystallisation behaviour through a nucleation effect and by changing the mobility of the polymer chain segments via a hindrance effect. If the chain mobility confinement effect is dominant during the crystallisation process, the crystallisation temperature shifts to lower values and the degree of crystallinity decreases. Otherwise, they increase due to heterogeneous crystallisation occurrence. In heterogonous crystallisation, CB particles act as nucleation agents that decrease the nucleation barrier energy for crystallisation and increase the crystallinity percentage.

It is clear from Fig. 5 and Table 3, that the crystallinity percentage of the composites are higher than the neat PP due to the heterogeneous crystallization of CB particles. However, regarding the competition between nucleation promotion and hindrance effect, the crystallinity degree increased up to the 2 wt.% CB and dropped at 3 wt.% CB due to the heterogeneous nucleation dominance and reduction of the chain mobility respectively. With increases in the CB loading the value of crystallinity changes due to a competition between nucleation promotion and hindrance effect.

An increase in crystallinity of the base material can contribute to an increase in the mechanical property of the overall laser-welded assembly. Therefore the weld strength of 1.0 wt.% CB composites could be higher compared to 0.5 wt.% CB. Also, higher crystallinity may lead to more scattering [31], resulting in wider WW and reduced weld depth. The addition of nucleating agents in the L_T layer can increase the percentage crystallinity as well as the degradation temperature. The samples can be welded at higher laser power values and faster welding

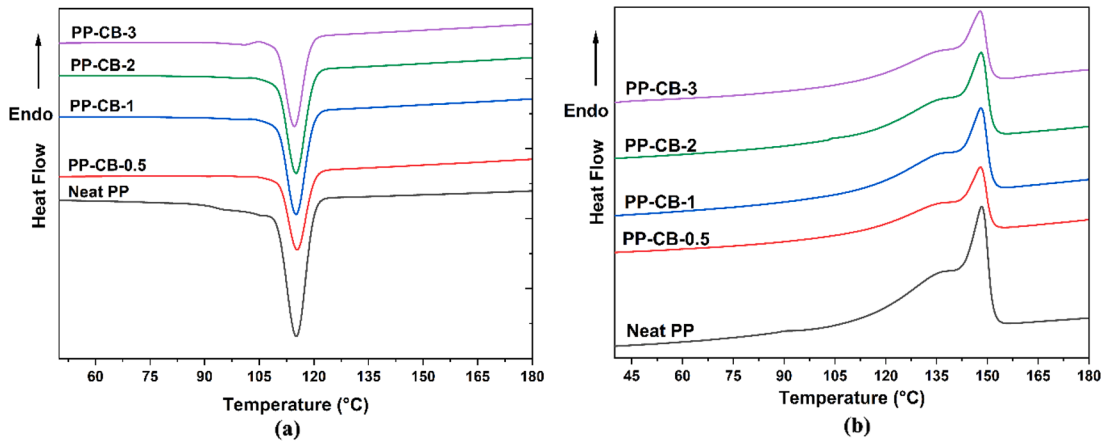

Fig. 4. DSC traces of iPP and its composites at 10° C/min under N_2 atm (a) cooling curve (b) second heating curve.

Table 3
DSC scan results (second heating curves): Effect of CB content on the melting behaviour and crystallinity.

Composite designation	Second endotherm (°C)		ΔH_f (J/g)	χ_{DSC} (%)
	T_{onset}	T_{m2}		
Neat PP	140.61	148.36	75.43	36.44
PP-CB-0.5	139.45	147.92	76.79	37.28
PP-CB-1	139.44	148.07	78.45	38.28
PP-CB-2	140.32	148.05	83.57	41.20
PP-CB-3	139.79	147.91	74.86	37.28

T_{onset} is thermoset temperature of melting, T_{m2} is the endothermic peak temperature/melting temperature, ΔH_f is the heat of fusion.

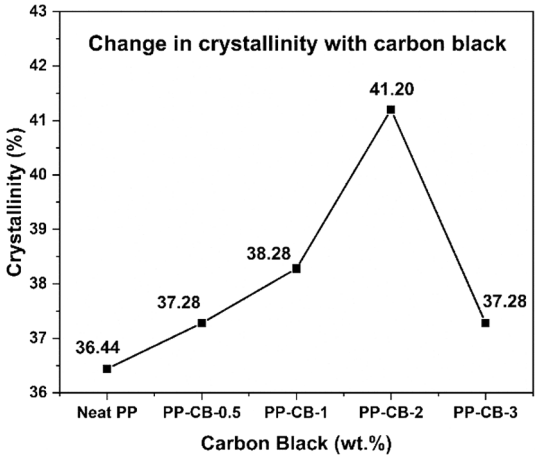

Fig. 5. Percentage crystallinity for iPP and its CB composites.

speed. However, the optical properties need to be taken care of, considering the scattering phenomenon leading to the loss of laser radiations.

3.2. Thermal modelling for design matrix

The thermal profiling of the lap joint area was carried out with the assistance of simulation modelling using the heat transfer module of COMSOL Multiphysics 5.6 software. The thermal model developed is a preliminary model which is only used to provide temperatures for the given laser process window. The details involving the analysis of the thermal profile of the lap joint area carried out are studied in the previously published work based on "Simulated Effect of Carbon Black on High-Speed Laser Transmission Welding of Polypropylene with Low Line Energy". Line energy is defined as the ratio of P and S. In order to calculate the temperature field, there were a few assumptions made with the help of the studies carried out by Acherjee et al. (2010) [32]. These are as follows:

1. The iPP and its composites are considered to be in close proximity and have isotropic thermophysical behaviour during the LTW process.
2. Conduction and convection mode of heat transfer was considered between the iPP and its CB composite and the phase transition heat effect were neglected.
3. The geometrical portion where the temperatures were higher than the material melt temperature (T_m) which were regarded as the weld zone.

The thermophysical and optical properties used in the simulation are provided in Table 4.

For the thermal simulation, the lap joint area has been used, as shown in Fig. 6 (a). Near the weld contour, mesh size was kept minimum and at the external boundaries of the geometry, the mesh size was kept larger, shown in Fig. 6 (b). By varying the P and S of the laser beam with a 2 mm spot diameter, the maximum weld temperature was calculated (Table 5). Based on the values of P and S, the obtained values of temperature greater than the polymer melting temperature (from DSC:>140 °C) and lesser than the degradation temperature (from TGA: <410 °C) were considered as a deciding factor for the welding input parameters [33]. The simulated thermal profile for the absorptive layer of 0.5 wt.% CB/iPP for P = 100 W, speed = 1200 mm/s at (0, y, z) plane during LTW at t = 0.025 s is shown in Fig. 6 (c) and thermal profile (temperature) of (x, y, 0) plane during LTW at t = 0.0127 s is shown in Fig. 6 (d).

Table 5 provides the information regarding the maximum temperature in the geometry, attained at weld contour for 0.5 wt.% and 1.0 wt.% CB. These simulated temperature values are considered approximations and bases for experiments for systematically reducing the number of trials and errors. The table indicates that for the given process window, the temperature attained was above the melting temperature (>140 °C). For certain combinations of S and P, the attainable temperatures were higher than the degradation temperature (>410 °C, section 3.1). However, composites at these combinations were feasible to weld leading to good welding during laser trial experiments. This is because the degradation temperatures were obtained from TGA analysis carried out at 20 °C/min, which was much slower than the S rate (S > 1000 mm/s). The polymer degradation is negligible at high S (rapid thermal cycle in welding), which implies the degradation percentage of the material to the overall weld is insignificant. Composites containing 2 and 3 wt.% CB

Table 4
Thermophysical and optical properties of iPP used in simulations.

Material	Density (kg.m^3)	Specific heat (J.g^{-1}.K^{-1})	Thermal conductivity (W.m^{-1}.K^{-1})	Extinction coefficient [1/mm]
iPP	900	$= \begin{cases} 1.92[1+3(T-25)10^{-3}] & for\ T \le T_m \\ 2.54[1+1.4(T-25)10^{-3}] & for\ T > T_m \end{cases}$	0.21	0.11
PP-CB-0.5	900	$= \begin{cases} 1.92[1+3(T-25)10^{-3}] & for\ T \le T_m \\ 2.54[1+1.4(T-25)10^{-3}] & for\ T > T_m \end{cases}$	0.23	35
PP-CB-1	900	$= \begin{cases} 1.92[1+3(T-25)10^{-3}] & for\ T \le T_m \\ 2.54[1+1.4(T-25)10^{-3}] & for\ T > T_m \end{cases}$	0.25	70

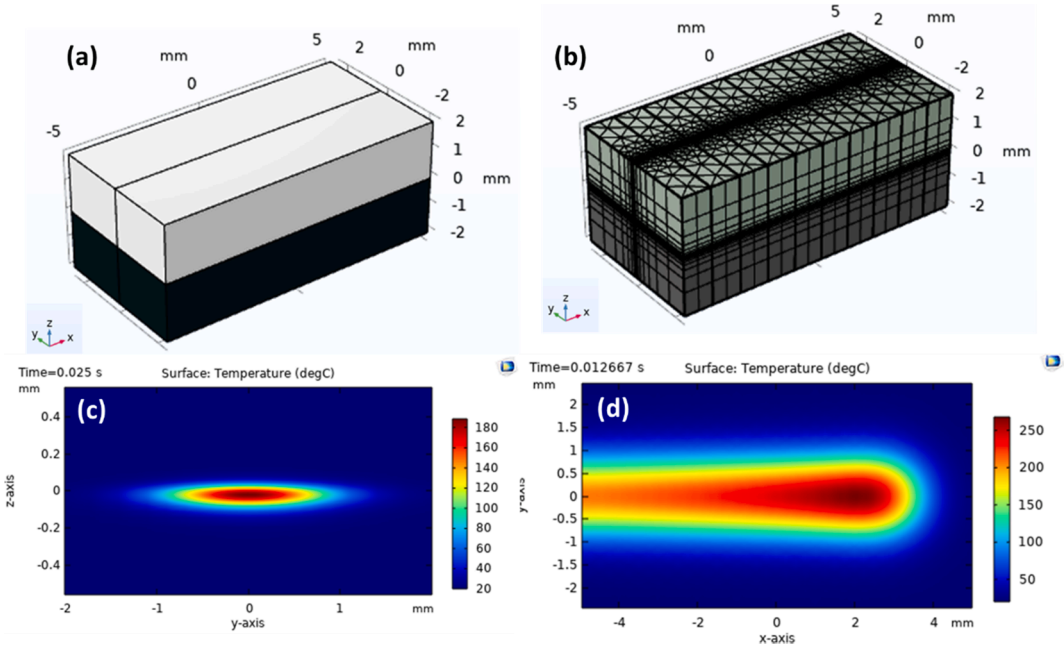

Fig. 6. (a) Schematics of LT and LA with wt.% CB with the lapped portion (b) An illustration of non-uniform pattern of mesh utilised for geometrical model (c) thermal profile (temperature) of (0, y, z) plane during LTW at t = 0.025 s (d) thermal profile (temperature) of (x, y, 0) plane during LTW at t = 0.0127 s of simulation for LA of 0.5 wt.% CB containing iPP for P = 100 W and S = 1200 mm/s.

Table 5
Simulated temperatures for the given process window.

Variables		0.5 wt.% CB		1.0 wt.% CB	
Laser power (P in Watt)	Welding speed (S in mm/s)	Boundary T_{max} (in °C)	T_{max} (in °C)	Boundary T_{max} (°C)	T_{max} (in °C)
80	1000	254	332	383	448
80	1200	222	293	338	398
80	1400	195	258	305	360
100	1000	306	402	461.5	540
100	1200	268	356	406.5	480
100	1400	239	320	367.5	434.5
120	1000	358	469	540	632
120	1200	313	416	475	562
120	1400	279	375	430	509

Tmax: Maximum temperature in the geometry.
Boundary T_{max}: Maximum temperature attained at weld contour.

could not be welded experimentally with the same set of parameters which will be discussed in the next section of the experimental design.

4. Experimental design

Contour laser welding was performed on an LPKF InlineWeld 6200 machine (Garben, Germany) with a spot diameter of 2.1 mm and clamping force of 700 N. Infrared radiations were produced by a high-power diode laser source with a wavelength of 980 nm (laser pulse frequency of the continuous wave). The uniform pressure was applied with a pneumatic clamping device for an enhanced flow of the molten plastic material into the microstructures. ProSet 3.0 and WeldPro Light software (version 1.168) were used for contour formation and welding, respectively. The laser power (P) value was verified using a laser power meter Fit-500 from Laser 2000. The picture of the high-power diode laser machine is shown in Supplementary Note 2, Fig. 1.

The dimensions of the sample and the lap joint geometry is presented in Fig. 7. The L_T overlaps 10 mm with the L_A so that the overall length of the joint sample was about 70 mm, and the total joint area was 10×10 mm^2 with the welding direction in the z-axis.

Thermal properties and thermal modelling results were used to define the laser welding parameters. They assisted in systematically reducing the number of trial and error and providing estimation for laser parameters. This allows the joining technique of LTW to move beyond trial-and-error methods to robust analytical methods. Various laser trials were carried out experimentally by fixing the welding speed (S) and varying the laser power (P) from 10 to 150 W. With S = 1000 mm/s and P < 80 W, there was no welding observed between L_T and L_A. This is because there is insufficient thermal energy to melt the thermoplastic at low P values or low line energy. The 0.5 wt.% and 1 wt.% CB containing composites were getting welded for P = 80–120 W and S = 1000 mm/s. Degradation was observed for P > 120 W for S = 1000 mm/s. Later, P was fixed to 120 W, and S was gradually increased from 1000 mm/s to 2000 mm/s. L_T and L_A were successfully welded until S = 1400 mm/s. For S > 1400 mm/s and P = 120 W, there was no welding observed again due to low line energy.

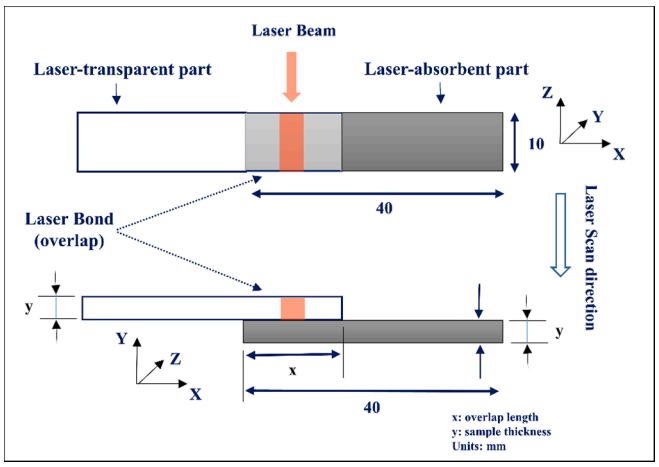

Fig. 7. Scheme of lap joint geometry with a top view (top) and side view (bottom).

In the present study, full quadratic Central Composite Design (CCD) of RSM was utilised (Table 1 of Supplementary Note 3 shows 52 experimental observations). The backward elimination process eliminated the terms that were not significant to improve the model's adequacy [9]. The low, mid and high levels of the continuous factors of design of experiment, P and S, are mentioned in Table 6 with units and notations. Two levels of CB were studied as categorical factors, 0.5 wt.% and 1.0 wt.% CB, as higher levels got degraded at the given laser processing condition. All other laser parameters were kept constant. The theory and advantages of using the RSM and ANOVA method are provided in detail in Supplementary Note 1.

Box-Behnken Design is also another approach that can be utilised for three factors at three levels. Although the method does require slightly fewer experiments to be performed compared to CCD, the quality of the prediction is poor near the extremes of the experimental domain.

A pneumatic clamping device applied a uniform pressure (clamping force 700 N) to enhance the molten plastic material in the microstructures. The composites were welded to obtain a smoother heat-affected zone (HAZ) as the first visual inspection reported by Juhl et al., 2013 [34], avoiding obvious material decomposition or other visual defects.

For the given process window in Table 6, laser trials for the composites containing 2.0 and 3.0 wt.% of CB were also carried out. However, these composites got degraded before they could melt for weld formation due to excess laser energy absorbed by the CB particles. Fig. 8 (a) and (b) show the neat iPP welded with the composite containing 0.5 wt.% CB and degraded with the 3.0 wt.% CB loaded composite.

5. Morphological characterisation

The thermal history of the polymers defines their morphologies, including changes in spherulitic structures, spherulitic size, crystallinity, etc. Hence, the thermal transition taking place during the LTW process can change the initial orientation of microstructures. The complete melting of the weld zone leads to recrystallisation initiating from the primary nucleation step leading to the growth of large spherulites. The region surrounding the weld zone undergoes partial melting with the

Table 6
Process control LTW parameters for welding composites, their limits and levels.

Factors	Variables	Unit	Notations	Levels		
				Low	Mid	High
Continuous	Laser power	W	P	80	100	120
	Welding speed	mm/s	S	1000	1200	1400
Categorical	Carbon Black	(%)	CB	0.5 and 1.0		

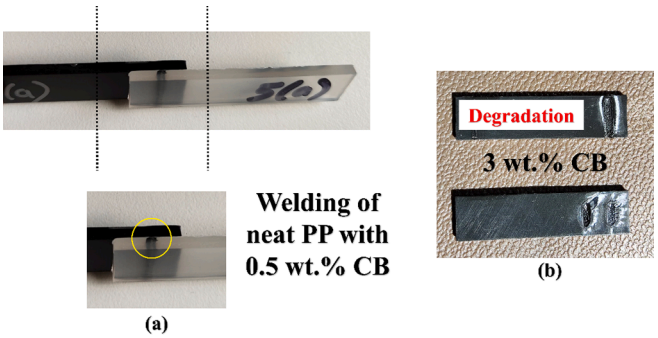

Fig. 8. Welding trials (a) Welding of neat iPP with 0.5 wt.% CB (b) Degradation of 3.0 wt.% of CB composites for the given process window.

combination of homogeneous (from the melted polymer), heterogeneous crystallisation (from the surface of the crystal) and secondary nucleation process occurs upon cooling. The overall change of the polymer morphology at the weld zone and its surrounding strongly influences the mechanical properties of the welded thermoplastic. It is difficult to study the morphological changes of the thermally treated thermoplastics through laser radiations once the samples are welded together. The non-contact spacer method was used to prepare laser-treated, and non-laser treated areas on samples to study the effect of laser process parameters or the thermal cycle on the crystallinity behaviour and type of crystals present in the samples using XRD. The samples containing 0.5 wt.% and 1 wt.% were considered for this study with neat iPP as the L_T layer. The laser treatment is not the exact replica of the welding of the samples due to a spacer in between; however, the observation of the change of crystallinity trend in the laser-treated samples has been considered an interesting insight.

As shown in Fig. 9, in the non-contact spacer method [34], a spacer of the thickness of 0.5 mm was placed above the L_A followed by L_T. The spacer prevents the welding of the two components. A series of line scans at various line energies were made at a constant S of 1000 mm/s and varying the P, i.e., 80 W, 100 W and 120 W.

Siemens D500 X-ray diffractometer operating at 40 kV and 30 mA using Cu-Kα radiation (λ = 1.5406 Å) was utilised to study the crystallinity behaviour of the laser-treated and non-laser-treated areas of the iPP samples [34]. Patterns were obtained over the range of 2-theta from 5° to 55° with an angular step interval of 0.02°. An aluminium holder was used for mounting the composites, and the height was adjusted using a glass slide. The crystallinity percentage was calculated from the ratio of crystalline peak area to the total peak area, as demonstrated by Bhadra et al. (2008) [35].

XRD analysis was carried out for the non-laser treated, and laser-treated composites after the non-contact spacer method were applied to composites. Fig. 10 (a) indicates the characteristics diffraction peaks

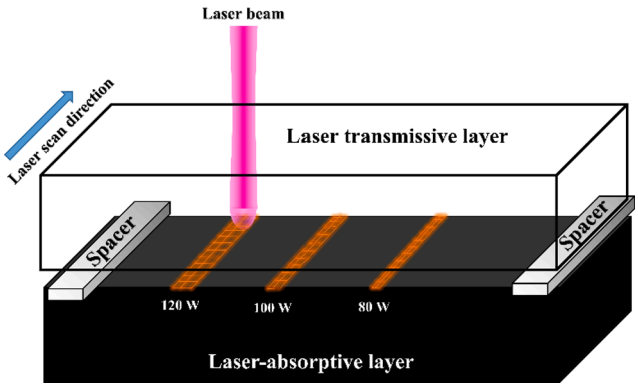

Fig. 9. Schematic representation of the non-contact spacer experiment set-up.

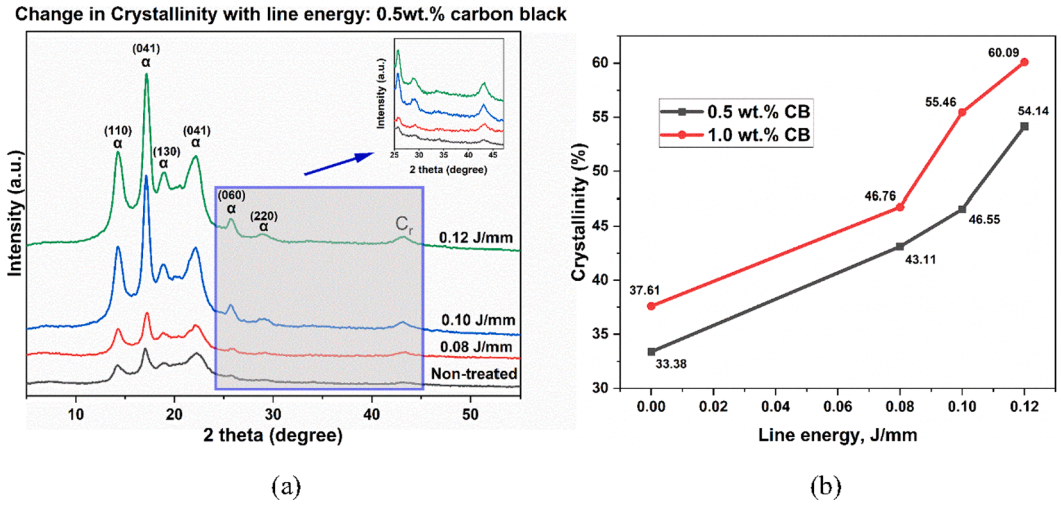

Fig. 10. (a) XRD traces of iPP and its CB composites show crystal peaks (example for 0.5 wt.% CB). (b) Increase in the percentage crystallinity with line energy and carbon black.

of $2\theta = 14.3°$, 17.2°, 18.8°, 22.2°, 25.7° and 28.7° correspond to the (1 1 0), (0 4 1), (1 3 0), (0 4 1), (0 6 0), and (2 2 0) planes respectively. The peaks represent the α – crystals of iPP, which was the dominant crystalline phase after a thermal modification [36-38]. The diffraction peak at 43°, denoted by C_r, was assigned to the (1 0 0) plane of CB [39-41]. It is apparent from Fig. 10 (b) that the intensity of the peaks and the percentage crystallinity increase with the line energy. The increase was higher for 1.0 wt.% CB compared to 0.5 wt.% CB. This can be attributed to the fact that with an increase in line energy, more heat is transferred to iPP chains, and chain scission occurs, which is more significant in iPP–CB composites. The chain scission decreases the number of chain entanglement and increases the motion ability of chains in the melted zone, which lead to an increased crystallinity percentage of iPP after resolidification [16]. The degree of crystallinity, spherulitic dimensions and its distribution determine the mechanical properties of iPP [42].

6. Mechanical testing and mathematical modelling

The mechanical testing was carried out for the laser-welded lap joint combination of neat iPP as L_T and 0.5 and 1 wt.% containing CB as L_A layer followed by their weld width measurements.

6.1. Weld width measurement

The weld widths (WW) of the fractured specimens were measured using an Olympus microscope (model BX51) to calculate apparent lap weld shear strength (s). The distance between the two outer bounds of the joint line at the middle point of the laser absorptive parts was measured as the WW after the lap shear testing. An average of the three measurements of weld widths, w1, w2 and w3, were taken as an average apparent WW. Weld area was calculated according to equation (2):

$$\text{Weld area} = \text{average apparent weld width} \times \text{width of the specimen} \quad (2)$$

6.2. Weld lap shear test

The test specimens were fixed in the grips of the testing machine such that the applied load coincided with the specimen's long axis (Fig. 11). The crosshead extension rate was set to load the joint at the rate of 8.3 to 9.7 MPa min^{-1} (as per the ASTM D3164) using a load cell of 5KN at a temperature of 16 °C. Weld quality was evaluated by measuring the σ obtained by normalising maximum force (F_{max}) at the break with the weld area.

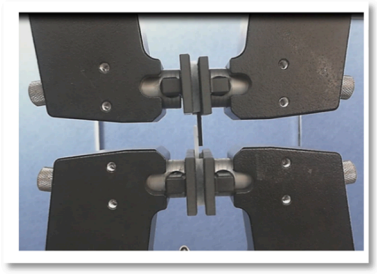

Fig. 11. Photograph of a lap shear welded composites between the clamps during a mechanical test.

Weld quality in laser transmission welding is a function of various properties: thermal, morphological, rheological, and optical. Multiple responses define weld quality. The present study determined the weld quality by mechanical testing of the welded assembly, with apparent WW (in mm) and σ (in MPa) as the responses. In lap shear testing, tension was applied at both the ends of the welding joints [43].

Weld lap shear strength (σ) was determined with the help of the following equation (3) taking ASTM D3164 as reference:

$$\text{Weld shear strength}(\sigma) = \frac{Fmax}{\text{Apparent weld width} \times \text{thickness}} \quad (3)$$

where F_{max} is the maximum force in N required for weld failure, as shown in Fig. 12 (a) load Vs extension graph. The distance between the two outer bounds of the joint line at the middle point of L_A was measured as apparent WW, as shown in Fig. 12 (b). F_{max} value for composite containing 1.0 wt.% CB (base material crystallinity 38.28%) was higher than 0.5 wt.% CB (base material crystallinity 37.28%) for a given laser parameter of P and S. The crystallinity of individual components will contribute to the overall mechanical property of the laser-welded assembly. A similar correlation of mechanical properties and crystallinity for base polymer was observed by Verma et al., 2015 [44] during shielding studies and again in [30] during the study of iPP random copolymer with varying carbon nanotubes (0, 0.2, 0.4, 0.9, 1.8 and 4.6 wt.%).

6.3. Development of mathematical models

The experiment was designed based on the two continuous factors, P and S, at three levels of CCD-RSM as shown in Table 1 of Supplementary

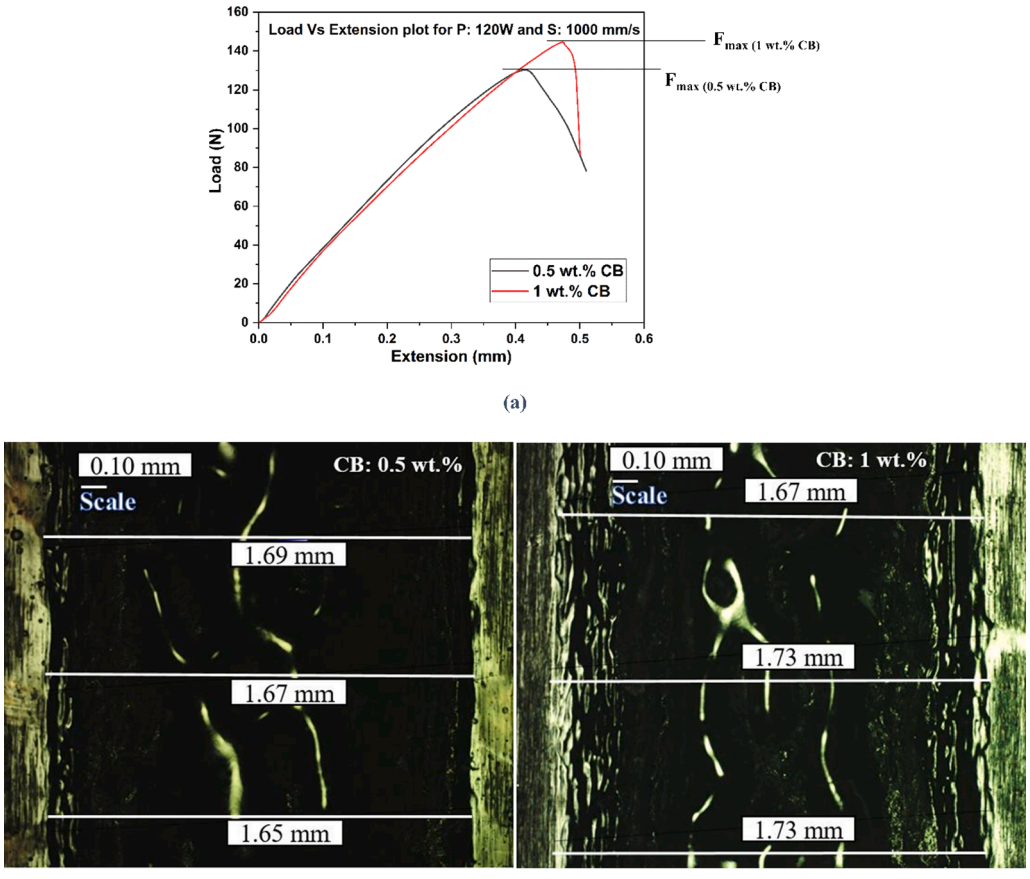

Fig. 12. iPP composite with 0.5 and 1.0 wt.% CB welded at laser power 120 W and welding speed 1000mm/s. (a) Load Vs extension graph (b) microscopic images of the apparent weld widths measured after lap shear testing.

Note 3, taking the 0.5 and 1.0 wt.% CB loaded composites as a categorical factor (2 and 3 wt.% CB loaded composites degraded). Face-centered was used with alpha = 1 and two replicates (blocks), making the total number of independent design points/ experiment = 52. The bond quality was evaluated by σ and apparent WW. According to the design matrix, the experiment was randomly carried out to avoid any systematic error in the investigation.

Minitab v19 software was used to analyse the measured responses and determine the mathematical models with the best fits. Supplementary Note 4 (Table 2) and 5 (Table 3) shows the ANOVA of the responses WW and σ, respectively. The backward elimination process eliminated the model terms associated with σ and WW responses, which were insignificant (significance criteria: p-value < 0.05; 95% confidence level). Quadratic regression equations (4–7) for predicting σ of 0.5 wt.% CB ($\sigma_{0.5\%\ CB}$) and 1.0 wt.% CB ($\sigma_{1\%\ CB}$) and apparent WW of 0.5 wt.% CB ($WW_{0.5\%\ CB}$) and 1.0 wt.% CB ($WW_{1\%\ CB}$) were obtained as follows:

$$WW_{0.5\%\ CB} = 1.512 - 0.00503P + 0.000335S + 0.000049P^2 - 0.000000263S^2 \quad (4)$$

$$WW_{1\%\ CB} = 1.535 - 0.00503P + 0.000335S + 0.000049P^2P - 0.000000263S^2 \quad (5)$$

$$\sigma_{0.5\%\ CB} = 10.78 - 0.01P - 0.006919S + 0.000959P^2 \quad (6)$$

$$\sigma_{1\%\ CB} = 11.46 - 0.0781P - 0.006919S + 0.000959P^2 \quad (7)$$

The F-value and the Pareto chart (Supplementary Note 4–7) were used to determine the relative significance of the input variables. Higher F-value indicates a more significant effect. The ANOVA table and the Pareto chart suggest that P was the most influencing input variable, followed by S and CB for WW and σ. The quadratic effect of P (P^2) was significant for σ and WW. Even the S (S2) quadratic effect was significant apart from P (P^2). The Pareto charts in Supplementary Notes 6 and 7 showed that P was more significant than S in influencing σ and WW. The predicted values of WW and S were calculated based on the regression equations 4–7. The correlation between the actual experimental values of WW and σ with predicted values is shown in Fig. 13 (a) and (b), respectively. The R^2 value for the plot for WW is 95.58%, and that for σ is 89.48%. The adequacy measures indicate an adequate model [45,46]. The figure shows that the obtained models for predicting the responses are appropriate and consistent with the actual experimental values.

7. Effect of line energy and carbon black on the responses

The size and shape of the welded specimen, internal stresses or flaws of the specimen during processing and the environmental factors determine σ. With an increase in P, a greater volume of the base material was melted; hence a wider weld-seam width is obtained. Similar observations were made by Kumar et al. (2021) [47] and Acherjee et al. (2009) [9] during the optimisation studies of LTW of thermoplastics. In the present study, the WW of the samples decreases at higher values of S. With an increase in S, interaction time/irradiation time between the laser beam and the material gets reduced. Consequently, the amount of heat delivered is also reduced. Samples welded at higher S values have morphology closer to the original iPP matrix morphology as the exposure to the thermal cycle was for a shorter period. The main effect plot for WW (Fig. 14) and σ (Fig. 15) versus the process parameters showed that the maximum value of the responses was achieved at higher P and

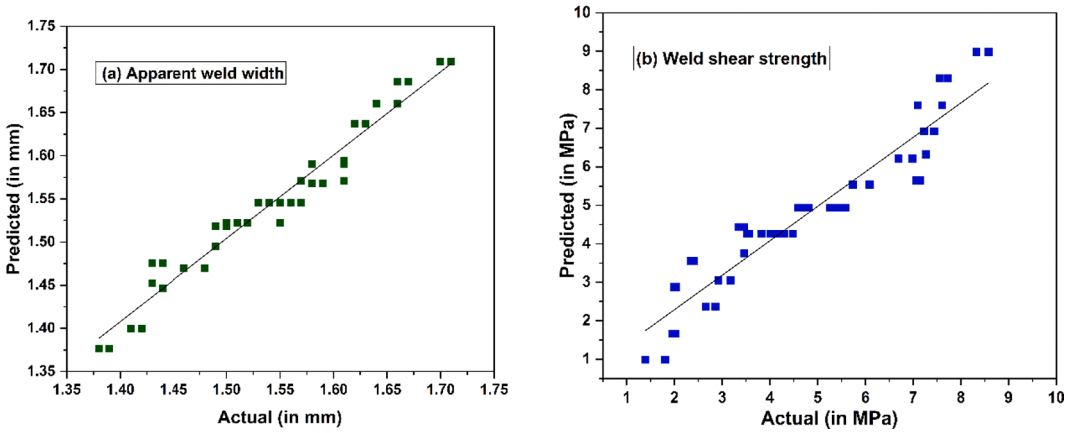

Fig. 13. A plot of actual Vs predicted response of (a) WW (b) σ results.

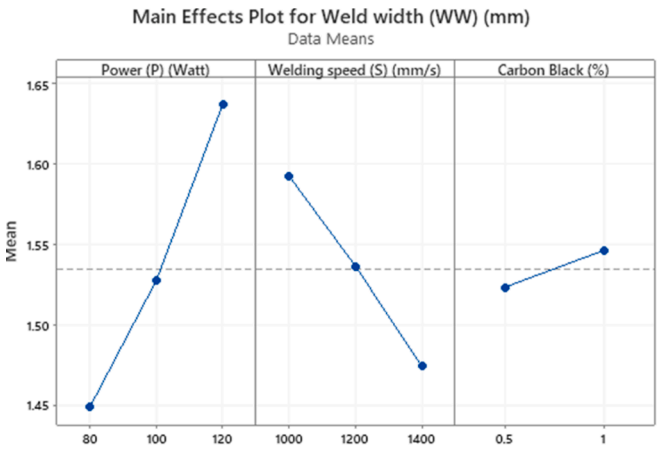

Fig. 14. Main effect plot of P, S and CB for weld width.

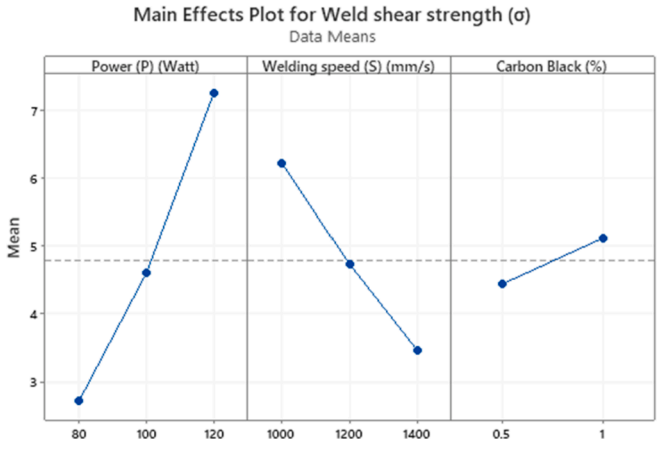

Fig. 15. Main effect plot of P, S and CB for weld shear strength.

CB at lower S values.

Due to an adequate clamp pressure (with clamping force 700 N), good contact between the overlapped specimens resulted in better heat conduction. During LTW studies, Liu et al. (2016) [48] and Russek et al. (2003) [49] observed that the mechanical properties are dependent on the line energy in addition to material properties (melting temperature, thermal conductivity, etc.). In the present study, the composites were welded at very low line energy ranging from 0.06 to 0.12 J/mm. Fig. 16 (a) and (b) shows the bar graph of the mean values of WW and σ at various line energies, depicting the effect of line energy and CB on the responses. It can be seen from the graph (Figs. 14 and 15) that WW and σ increase with an increase in the line energy. At lower line energy (lower P and higher S), there is poor heat transfer which may not be sufficient for the material to completely melt and flow, resulting in inadequate material inter-diffusion and no welding of the parts. The WW and σ increase was higher for the composite containing a greater percentage of CB, i.e., 1.0 wt.% CB > 0.5 wt.% CB. This is due to a higher percentage of crystallinity of the sample containing 1.0 wt.% CB (38.28%) than that of 0.5 wt.% (37.28 %) as discussed in section 3.1 obtained through DSC results. Also, based on the XRD results of morphological studies (section 5) from the non-contact spacer method, it was observed that the recrystallisation during the resolidification after laser treatment led to a higher percentage of crystallinity of the sample containing 1.0 wt.% CB compared to 0.5 wt.% CB. A greater variation was observed on the Thermo-mechanical performance at 0.5 wt.% CB due to volumetric heat generation. According to the literature, there may be a generation of higher van der Waals forces at higher line energy and an improved weld strength [50] with more material being melted, resulting in a wider WW.

Higher S leads to low-heat input of the base material; as a result, σ decreases. However, at lower speed and higher P values, the material can burn and eventually decompose. An optimum value of weld strength can be attained at a favourable value of line energy with an appropriate combination of P and S.

8. Optimisation of weld width and weld lap shear strength

In order to maximise WW and σ, response optimisation was carried out for 0.5 wt.% and 1.0 wt.% CB values. The column in Fig. 17 represents the process parameter, and the row represents a response variable. Each cell of the optimisation plot represents how one of the responses varies as a function of laser process parameters with other parameters constant [51]. The numbers at the top of each column show the upper and lower levels of the laser process parameters as well as the optimum parameter level. The first column of each row shows the target of responses and response predicted to achieve the target (y) at the optimum parametric setting.

It was found from the optimisation plot that for P = 120 W, S = 1000 mm/s and 1.0 wt.% CB, the responses were maximised at WW = 1.7 mm and σ = 8.98 MPa. The experimental value obtained for maximum σ during the experiment for WW was 1.7 mm, and that for σ was 8.33 MPa in the case of 1 wt.% CB (Table 1, Supplementary Note 3). This indicates that the model obtained in the previous section for WW was a good fit with $R^2 = 95.58\%$ and for the σ model with $R^2 = 89.48\%$.

Considering the material aspects in the present study, the absorption coefficient of L_A increases with an increase in the CB content. An increased S with lower P can be used for composites containing higher

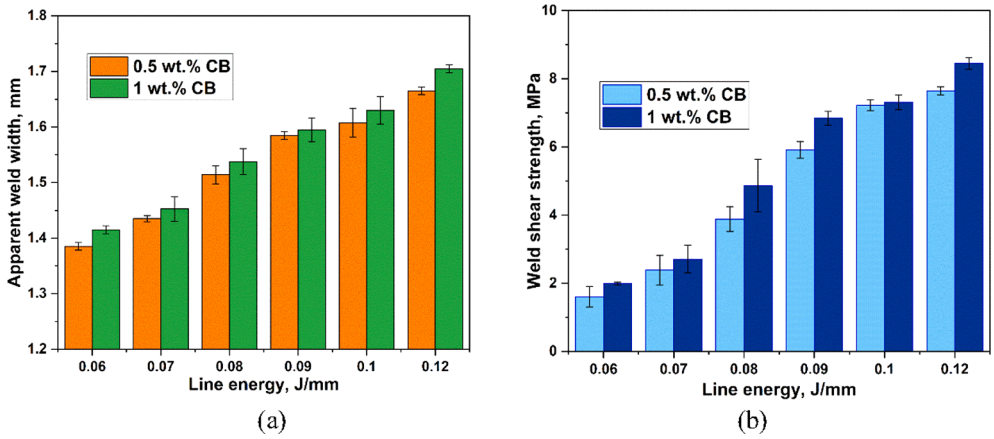

Fig. 16. Comparison of (a) apparent weld width and (b) weld shear strength for 0.5 wt.% CB and 1.0 wt.% CB with line energy.

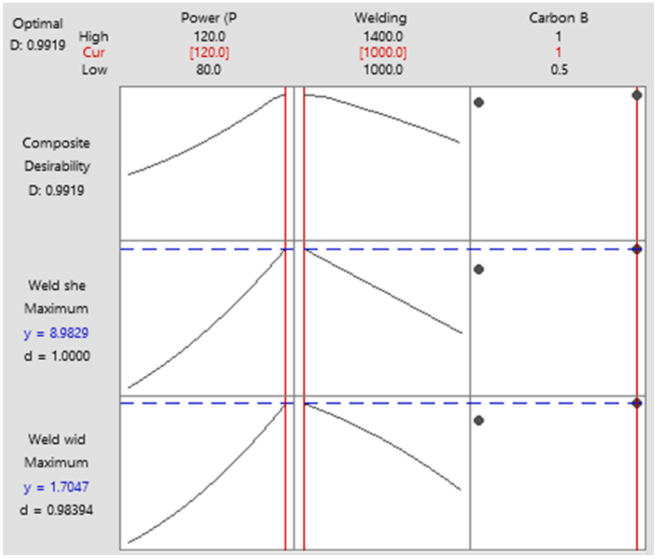

Fig. 17. Optimisation plot for weld width and weld lap shear strength.

CB. Higher CB would change the absorption type: from volume absorption to surface absorption. Since the radiant energy gets absorbed over a broad layer of absorbing material in volume absorption, the temperature attained at the interface was relatively low, resulting in narrow WW in $L_{A,}$ i.e., higher optical penetration depth. The radiant energy gets completely absorbed in a very thin layer of the laser absorbing part in surface absorption. As the absorbed energy gets converted into heat at the surface, the interface reaches a higher temperature, resulting in a wider WW and a reduced penetration depth. This was also observed by Acherjee et al., 2012 [52] during model development for LTW and again in 2012 [53] while studying the effect of carbon black during LTW of polymers. CB content affects the WW more strongly than weld depths in L_T and L_A.

9. Conclusion

iPP-CB composite samples (0.5 wt.% and 1.0 wt.%) were successfully welded with the neat iPP composites at low line energy of 0.06–0.12 J/mm using the diode laser transmission welding machine. With the same processing window, the composites containing a higher percentage of CB (>1.0 wt.%) could not be welded. Melting temperature and decomposition temperature obtained from thermal characterisation and laser temperatures for the given parameters obtained from thermal simulation facilitated defining an estimation of the laser process window. Central Composite Design was utilised with backward elimination for optimising the weld quality in terms of apparent weld width and weld lap shear strength. The primary conclusions drawn from the thermal, morphological and mechanical characterisation are as follows:

- Carbon black concentration plays a significant role in the laser transmission welding process for achieving better weld quality. With an increase in CB, the type of absorption changes from volume absorption to surface absorption. At 1 wt.% CB, the temperature profile and the mechanical performance of the welds were more stable compared to 0.5 wt.% CB.
- Crystallinity also plays an essential role in defining weld integrity and weld quality. The percentage of crystallinity of the base material increased with an increase in CB content up to 2.0 wt.% CB. For 3.0 wt.% CB, there was a decrease in the percentage crystallinity.
- A novel approach of a non-contact spacer method facilitated the study of the crystallinity trend in detail for laser-treated composites through XRD. This approach was used to study the morphological changes in the polymer due to thermal transitions occurring during LTW. With an increase in line energy and percentage of CB content, there was an increase in the iPP crystallinity. For a given line energy treatment of 0.12 J/mm, the crystallinity for 0.5 wt.% CB was 54.14%, and that of 1.0 wt.% CB was 60.09%. An increase in crystallinity of the laser treated base material contributed to the overall increase in the weld strength of the laser-welded composite.
- ANOVA results and the Pareto chart (supplementary Note 4–7) indicated that both P and S have more substantial effects on WW and σ, with P being the most significant factor. The main effect plot showed that increasing P increased WW and σ, whereas increasing S decreased both the responses. The responses were maximised at an optimised value of 120 W, 1000 mm/s and 1.0 wt.% CB. As the responses are very sensitive to the laser process parameters, selecting the parameters needs to be carried out systematically.
- The predicted values obtained through regression equations were in good agreement with the experimental data. Hence, the model can predict WW and σ effectively within the limits of laser welding parameters being used.

The correlation of CB affecting polymer crystallinity and the dependency of mechanical properties of laser-welded joints on crystallinity is well established in the present study. However, further studies on understanding the correlation of different zones in the welded area with the crystalline morphology could assist in getting more deeper insights into the polymer microstructure modification and its evolution with varying laser parameters and CB compositions. Composites with higher wt.% CB could potentially be welded at lower P and higher S as part of future work. The thermal exposure time for the material at welding

speed is very low compared to that during thermal characterisation. If the correlation of these heating rates is studied in detail, it can further reduce the number of experimental trials to set the laser processing window. With the help of Avrami's equation, the rate of crystallisation can be determined along with the nucleation and growth parameter. The simulation model can also be developed further to predict the location of degradation during the LTW process.

Funding

This research was funded by The North West Centre for Advanced Manufacturing (NWCAM) project is supported by the European Union's INTERREG VA Programme, managed by the Special EU Programmes Body (SEUPB).

CRediT authorship contribution statement

Foram Dave: Conceptualization, Methodology, Formal analysis, Investigation, Writing – original draft, Writing – review & editing. **Muhammad Mahmood Ali:** Software, Writing – review & editing. **Mozaffar Mokhtari:** Foraml analysis, Visualization, Writing – review & editing. **Richard Sherlock:** Resources, Supervision, Project administration, Funding acquisition, Writing – review & editing. **Alistair McIlhagger:** Resources, Supervision, Project administration, Funding acquisition, Writing – review & editing. **David Tormey:** Resources, Supervision, Project administration, Funding acquisition, Writing – review & editing.

Declaration of Competing Interest

The authors declare that they have no known competing financial interests or personal relationships that could have appeared to influence the work reported in this paper.

Acknowledgements

The North-West Centre for Advanced Manufacturing (NWCAM) project is supported by the European Union's INTERREG VA Programme, managed by the Special EU Programmes Body (SEUPB). The views and opinions in this document do not necessarily reflect those of the European Commission or the Special EU Programmes Body (SEUPB). If you would like further information about NWCAM, please contact the lead partner, Catalyst Inc, for details. Mark Mcloughlin is acknowledged for tool designing.

Data Availability Statement

The raw data supporting the conclusions of this article are available from the corresponding author upon reasonable request

Appendix A. Supplementary data

Supplementary data to this article can be found online at https://doi.org/10.1016/j.optlastec.2022.108216.

References

[1] B. Acherjee, Laser transmission welding of polymers – a review on process fundamentals, material attributes, weldability, and welding techniques, J. Manuf. Process. 60 (October) (2020) 227–246, https://doi.org/10.1016/j.jmapro.2020.10.017.
[2] B. Acherjee, State-of-art review of laser irradiation strategies applied to laser transmission welding of polymers, Opt. Laser Technol. 137 (August) (2020) 2021, https://doi.org/10.1016/j.optlastec.2020.106737.
[3] B. Cosson, M. Deléglise, W. Knapp, Numerical analysis of thermoplastic composites laser welding using ray tracing method, Compos. Part B Eng. 68 (2015) 85–91, https://doi.org/10.1016/j.compositesb.2014.08.028.
[4] M. Aden, Influence of the Laser-Beam Distribution on the Seam Dimensions for Laser-Transmission Welding: A Simulative Approach, Lasers Manuf. Mater. Process. 3 (2) (2016) 100–110, https://doi.org/10.1007/s40516-016-0023-x.
[5] M.S. Brown, et al., Numerical model of CO2 laser welding of thermoplastic polymers, J. Laser Appl. 32 (1) (2007), 022004, https://doi.org/10.1177/0731684413489755.
[6] A.M. Visco, N. Campo, L. Torrisi, A. Borrielli, Polyethylene film welding induced by a 532nm pulsed laser, Radiation Effects and Defects in Solids 165 (6–10) (Jun. 2010) 601–608, https://doi.org/10.1080/10420151003729458.
[7] D. Kumar, N.S. Sarkar, B. Acherjee, A.S. Kuar, Beam wobbling effects on laser transmission welding of dissimilar polymers: Experiments, modeling, and process optimization, Opt. Laser Technol. 146 (July) (2021) 2022, https://doi.org/10.1016/j.optlastec.2021.107603.
[8] P. Jaeschke, D. Herzog, H. Haferkamp, C. Peters, A.S. Herrmann, Laser transmission welding of high-performance polymers and reinforced composites - A fundamental study, J. Reinf. Plast. Compos. 29 (20) (2010) 3083–3094, https://doi.org/10.1177/0731684410365365.
[9] B. Acherjee, D. Misra, D. Bose, K. Venkadeshwaran, Prediction of weld strength and seam width for laser transmission welding of thermoplastic using response surface methodology, Opt. Laser Technol. 41 (8) (2009) 956–967, https://doi.org/10.1016/j.optlastec.2009.04.007.
[10] B. Acherjee, A.S. Kuar, S. Mitra, D. Misra, Selection of Process Parameters for Optimizing the Weld Strength in Laser Transmission Welding of Acrylics, Proc. Inst. Mech. Eng., Part B: J. Eng. Manuf. 224 (10) (2010) 1529–1536.
[11] E. Haberstroh, R. Lützeler, Influence of carbon black pigmentation on the laser beam welding of plastics micro parts, J. Polym. Eng. 21 (2–3) (2001) 119–130, https://doi.org/10.1515/POLYENG.2001.21.2-3.119.
[12] E. Haberstroh, W.M. Hoffmann, R. Poprawe, F. Sari, 3 Laser transmission joining in microtechnology, Microsyst. Technol. 12 (7) (Feb. 2006) 632–639, https://doi.org/10.1007/s00542-006-0096-0.
[13] M. Chen, G. Zak, P.J. Bates, Effect of carbon black on light transmission in laser welding of thermoplastics, J. Mater. Process. Technol. 211 (1) (2011) 43–47, https://doi.org/10.1016/j.jmatprotec.2010.08.017.
[14] Y. Kong, J.N. Hay, The measurement of the crystallinity of polymers by DSC, Polymer (Guildf) 43 (14) (2002) 3873–3878, https://doi.org/10.1016/S0032-3861(02)00235-5.
[15] M. Mucha, J. Marszałek, A. Fidrych, Crystallization of isotactic polypropylene containing carbon black as a filler, Polymer (Guildf) 41 (11) (May 2000) 4137–4142, https://doi.org/10.1016/S0032-3861(99)00706-5.
[16] E. Ghorbel, G. Casalino, S. Abed, Laser diode transmission welding of polypropylene: Geometrical and microstructure characterisation of weld, Mater. Des. 30 (7) (2009) 2745–2751, https://doi.org/10.1016/j.matdes.2008.10.027.
[17] M. Mokhtari, E. Archer, N. Bloomfield, E. Harkin-Jones, A. McIlhagger, High-performance and cost-effective melt blended poly(ether ether ketone)/expanded graphite composites for mass production of antistatic materials, Polym Int 70 (8) (2021) 1137–1145.
[18] F. Dave, M.M. Ali, R. Sherlock, A. Kandasami, D. Tormey, Laser Transmission Welding of Semi-Crystalline Polymers and Their Composites: A Critical Review, Polymers 13 (5) (2021) 675, https://doi.org/10.3390/polym13050675.
[19] N. Amanat, C. Chaminade, J. Grace, D.R. McKenzie, N.L. James, Transmission laser welding of amorphous and semi-crystalline poly-ether-ether-ketone for applications in the medical device industry, Mater. Des. 31 (10) (2010) 4823–4830, https://doi.org/10.1016/j.matdes.2010.04.051.
[20] R. Prabhakaran, M. Kontopoulou, G. Zak, P.J. Bates, B.K. Baylis, Contour laser - Laser-transmission welding of glass reinforced nylon 6, J. Thermoplast. Compos. Mater. 19 (4) (2006) 427–439, https://doi.org/10.1177/0892705706062200.
[21] B. Acherjee, Laser transmission welding of polymers – a review on welding parameters, quality attributes, process monitoring, and applications, J. Manuf. Process. 64 (February) (2021) 421–443, https://doi.org/10.1016/j.jmapro.2021.01.022.
[22] B. Acherjee, Hybrid laser arc welding: State-of-art review, Opt. Laser Technol. 99 (2018) 60–71, https://doi.org/10.1016/j.optlastec.2017.09.038.
[23] B. Acherjee, Selection of optimal parameters for laser transmission welding of polycarbonate using desirability function analysis, Mater. Today Proc. 4 (8) (2017) 7161–7170, https://doi.org/10.1016/j.matpr.2017.07.042.
[24] V. Mamuschkin, A. Roesner, M. Aden, Laser transmission welding of white thermoplastics with adapted wavelengths, Phys. Procedia 41 (2013) 172–179, https://doi.org/10.1016/j.phpro.2013.03.067.
[25] X. Wang, D. Guo, G. Chen, H. Jiang, D. Meng, Z. Yan, H. Liu, Thermal degradation of PA66 during laser transmission welding, Opt. Laser Technol. 83 (2016) 35–42, https://doi.org/10.1016/j.optlastec.2016.02.022.
[26] E. Rodríguez-Vidal, J. Lambarri, C. Soriano, C. Sanz, G. Verhaeghe, A combined experimental and numerical approach to the laser joining of hybrid polymer - Metal parts, Phys. Procedia 56 (C) (2014) 835–844, https://doi.org/10.1016/j.phpro.2014.08.101.
[27] K. Chrissafis, K.M. Paraskevopoulos, S.Y. Stavrev, A. Docoslis, A. Vassiliou, D. N. Bikiaris, Characterization and thermal degradation mechanism of isotactic polypropylene/carbon black nanocomposites, Thermochim. Acta 465 (1–2) (2007) 6–17, https://doi.org/10.1016/j.tca.2007.08.007.
[28] Y. Mubarak, P.J. Martin, E. Harkin-Jones, Effect of nucleating agents and pigments on crystallisation, morphology, and mechanical properties of polypropylene, Plast. Rubber Compos. Process. Appl. 29 (7) (2000) 307–315, https://doi.org/10.1179/146580100101541111.
[29] K. Cho, F. Li, J. Choi, Crystallization and melting behavior of polypropylene and maleated polypropylene blends, Polymer (Guildf) 40 (7) (1999) 1719–1729, https://doi.org/10.1016/S0032-3861(98)00404-2.

[30] P. Verma, V. Choudhary, Polypropylene random copolymer/MWCNT nanocomposites: Isothermal crystallization kinetics, structural, and morphological interpretations, J. Appl. Polym. Sci. 132 (13) (2015) n/a–n/a, https://doi.org/10.1002/app.41734.
[31] R. Ma, B.o. Zhu, Q. Zeng, P. Wang, Y. Wang, C. Liu, C. Shen, Melt-processed poly (ether ether ketone)/carbon nanotubes/montmorillonite nanocomposites with enhanced mechanical and thermomechanical properties, Materials (Basel) 12 (3) (2019) 525, https://doi.org/10.3390/ma12030525.
[32] B. Acherjee, A. Kuar, S. Mitra, D. Mitra, Finite element simulation of laser transmission welding of dissimilar materials between polyvinylidene fluoride and titanium, Int. J. Eng. Sci. Technol. 2 (4) (2010) 176–186, https://doi.org/10.4314/ijest.v2i4.59285.
[33] M.M. Ali, F. Dave, R. Sherlock, A. Mcilhagger, D. Tormey, Simulated Effect of Carbon Black on High Speed Laser Transmission Welding of Polypropylene With Low Line Energy, Front. Mater. (Sep. 2021) 407, https://doi.org/10.3389/FMATS.2021.737689.
[34] M. Chen, G. Zak, P.J. Bates, Estimating contour laser transmission welding start-up conditions using a novel non-contact method, Weld. World 52 (11–12) (2008) 71–76, https://doi.org/10.1007/BF03266684.
[35] S. Bhadra, D. Khastgir, Determination of crystal structure of polyaniline and substituted polyanilines through powder X-ray diffraction analysis, Polym. Test. 27 (7) (2008) 851–857, https://doi.org/10.1016/j.polymertesting.2008.07.002.
[36] A. Gradys, P. Sajkiewicz, A.A. Minakov, S. Adamovsky, C. Schick, T. Hashimoto, K. Saijo, Crystallization of polypropylene at various cooling rates, Mater. Sci. Eng. A 413-414 (2005) 442–446, https://doi.org/10.1016/j.msea.2005.08.167.
[37] M.M. Favaro, M.C. Branciforti, R.E.S. Bretas, A X-ray study of β-phase and molecular orientation in nucleated and non-nucleated injection molded polypropylene resins, Mater. Res. 12 (4) (2009) 455–464, https://doi.org/10.1590/S1516-14392009000400014.
[38] C.H.S. Souza Rosa, M.G. Mothé, M.F. Vieira Marques, C.G. Mothé, S.N. Monteiro, Steam-exploded fibers of almond tree leaves as reinforcement of novel recycled polypropylene composites, J. Mater. Res. Technol. 9 (5) (2020) 11791–11800, https://doi.org/10.1016/j.jmrt.2020.08.069.
[39] M.H.M.T. Assumpção, R.F.B. De Souza, D.C. Rascio, J.C.M. Silva, M.L. Calegaro, I. Gaubeur, T.R.L.C. Paixão, P. Hammer, M.R.V. Lanza, M.C. Santos, A comparative study of the electrogeneration of hydrogen peroxide using Vulcan and Printex carbon supports, Carbon N. Y. 49 (8) (2011) 2842–2851, https://doi.org/10.1016/j.carbon.2011.03.014.
[40] F.C. Vicentini, P.A. Raymundo-Pereira, B.C. Janegitz, S.A.S. Machado, O. Fatibello-Filho, Nanostructured carbon black for simultaneous sensing in biological fluids, Sensors Actuators, B Chem. 227 (2016) 610–618, https://doi.org/10.1016/j.snb.2015.12.094.
[41] M. Carmo, A.R. dos Santos, J.G.R. Poco, M. Linardi, Physical and electrochemical evaluation of commercial carbon black as electrocatalysts supports for DMFC applications, J. Power Sources 173 (2) (2007) 860–866, https://doi.org/10.1016/j.jpowsour.2007.08.032.
[42] X. Zhang, D. Zhang, T. Liu, Influence of Nucleating Agent on Properties of Isotactic Polypropylene, Energy Procedia 17 (2012) 1829–1835, https://doi.org/10.1016/j.egypro.2012.02.319.
[43] H. Liu, Y. Jiang, W. Tan, X. Wang, Enhancement of the Laser Transmission Weldability between Polyethylene and Polyoxymethylene by Plasma Surface Treatment, Materials 11 (1) (2017) 29, https://doi.org/10.3390/ma11010029.
[44] P. Verma, P. Saini, R.S. Malik, V. Choudhary, Excellent electromagnetic interference shielding and mechanical properties of high loading carbon-nanotubes/polymer composites designed using melt recirculation equipped twin-screw extruder, Carbon N. Y. 89 (2015) 308–317, https://doi.org/10.1016/j.carbon.2015.03.063.
[45] J.A. Guzmán Torres, F.J. Domínguez Mota, E.M. Alonso-Guzmán, W. Martínez-Molina, J.G. Tinoco Ruiz, H.L. Chavez-Garcia, M.A. Navarrete Seras, M. Arreola Sánchez, Prediction of the tensile strength and electrical resistivity of concrete with organic polymer and their influence on carbonation using data science and a machine learning technique, Key Eng. Mater. 862 (2020) 72–77, https://doi.org/10.4028/www.scientific.net/KEM.862.72.
[46] E.M. Anawa, A.G. Olabi, Optimization of tensile strength of ferritic/austenitic laser-welded components, Opt. Lasers Eng. 46 (8) (2008) 571–577, https://doi.org/10.1016/j.optlaseng.2008.04.014.
[47] D. Kumar, S. Ghosh, A.S. Kuar, N. Maity, "Enhancement of Laser Transmission Welds in Acrylic and Polypropylene Copolymer (PPCP) Using Snap Drift Cuckoo Search (SDCS), Optimization" 49 (2021) 205–225.
[48] H. Liu, W. Liu, X. Zhong, B. Liu, D. Guo, X. Wang, Modeling of laser heat source considering light scattering during laser transmission welding, Mater. Des. 99 (2016) 83–92, https://doi.org/10.1016/j.matdes.2016.03.052.
[49] U.A. Russek, et al., Laser beam welding of thermoplastics, Proc. SPIE - Int. Soc. Opt. Eng. 4977 (Jul. 2003) 458–472, https://doi.org/10.1117/12.478606.
[50] C. Huang, Y.Y. Gao, H.X. Liu, H. Chen, P. Li, X. Wang, Multi-Factors Interaction Effects of Process Parameters on the Joint Strength of Laser Transmission Joining between PC and PA66, Key Eng. Mater. 579–580 (2013) 91–96, https://doi.org/10.4028/www.scientific.net/kem.579-580.91.
[51] N. Kumar, R. Sherlock, D. Tormey, Prediction of weld interface depth and width at optimum laser welding temperature for polypropylene, Procedia CIRP 81 (2019) 1272–1277, https://doi.org/10.1016/j.procir.2019.03.306.
[52] B. Acherjee, A.S. Kuar, S. Mitra, D. Misra, Modeling of laser transmission contour welding process using FEA and DoE, Opt. Laser Technol. 44 (5) (2012) 1281–1289, https://doi.org/10.1016/j.optlastec.2011.12.049.
[53] B. Acherjee, A.S. Kuar, S. Mitra, D. Misra, Effect of carbon black on temperature field and weld profile during laser transmission welding of polymers: A FEM study, Opt. Laser Technol. 44 (3) (2012) 514–521, https://doi.org/10.1016/j.optlastec.2011.08.008.